CRYSTAL STRUCTURE OF PLANT ACETOHYDROXYACID SYNTHASE, THE TARGET FOR SEVERAL COMMERCIAL HERBICIDES.

Mario Daniel Garcia[1], Jian-Guo Wang[2]*, Thierry Lonhienne[1], Luke William Guddat[1]*.

Article type : Original Articles

[1]School of Chemistry and Molecular Biosciences, The University of Queensland, Brisbane, Australia.

[2]State-Key Laboratory and Institute of Elemento-Organic Chemistry, National Pesticide Engineering Research Center and College of Chemistry, Nankai University, Tianjin, China.

Corresponding authors:

Luke Guddat, School of Chemistry and Molecular Biosciences, Building 76, The University of Queensland, Brisbane, QLD, 4072, Australia. Tel: +617 33563549. Fax: +617 33654699 E-mail: luke.guddat@uq.edu.au

Jian-Guo Wang, State-Key Laboratory and Institute of Elemento-Organic Chemistry, Nankai University, Tianjin, 300071, China Email: nkwjg@nakai.edu.cn

This article has been accepted for publication and undergone full peer review but has not been through the copyediting, typesetting, pagination and proofreading process, which may lead to differences between this version and the Version of Record. Please cite this article as doi: 10.1111/febs.14102

Running Title: Structure Of Plant Acetohydroxyacid Synthase

Abbreviations: Acetohydroxyacid synthase, AHAS; flavin adenine dinucleotide, FAD; thiamine diphosphate, ThDP; *Saccharomyces cerevisiae*, *Sc*; *Arabidopsis thaliana*, *At*; hydroxyethyl, HE; rmsd, root mean square deviation; *Escherichia coli*glyoxylate carboligase, *Ec*GCL; *Lactobacillus plantarum* pyruvate oxidase*, Lp*POX; pyruvate oxidase, POX; benzylformate decarboxylase, BFDC; Luria-Bertani, LB; Terrific Broth, TB; 2-(*N*-cyclohexylamino)ethanesulfonic acid, CHES;

Database: The coordinates and structure factors for uninhibited *At*AHAS have been deposited in the Protein Data Bank (www.pdb.org) with the PDB ID code 5K6Q.

Keywords: acetohydroxyacid synthase, acetolactate synthase, herbicide, inhibitor, ThDP.

Conflict of interest: None of the authors have a conflict of interest.

ABSTRACT (150 words)

Acetohydroxyacid synthase (AHAS, E.C. 2.2.1.6) is the first enzyme in the branched-chain amino acid biosynthesis pathway. Five of the most widely used commercial herbicides (*i.e.* sulfonylureas, imidazolinones, triazolopyrimidines, pyrimidinyl-benzoates and sulfonylamino-cabonyl-triazolinones) target this enzyme. Here we have determined the first crystal structure of a plantAHAS in the absence of any inhibitor (2.9 Å resolution) and itshows that the herbicide-binding site adopts a folded state even in the absence of an inhibitor. This is

unexpected because the equivalent regions for herbicide bindingin uninhibited *Saccharomyces cerevisiae* AHAS crystal structures are either disordered,or adopt a different fold when the herbicide is not present. In addition, the structure provides anexplanation as to why some herbicides are more potent inhibitorsof*Arabidopsis thaliana* AHAS compared to AHASs from other species (*e.g.Saccharomyces cerevisiae).* The elucidation of the native structure of plant AHAS provides a new platform for future rational structure-based herbicide design efforts.

INTRODUCTION

Acetohydroxyacid synthase (AHAS, E.C. 2.2.1.6) also known as acetolactate synthase is the first enzyme in the branched-chain amino acid (valine, leucine and isoleucine) biosynthesis pathway. Its function is to convert two molecules of pyruvate into (*S*)-2-acetolactate, or to convert one molecule of pyruvate and one molecule of 2-ketobutyrate into (*S*)-2-aceto-2-hydroxybutyrate. This activity is dependent on the presence of three cofactors, *i.e.* flavin adenine dinucleotide (FAD), thiamine diphosphate (ThDP), and magnesium ion (Mg^{2+}) [1]. AHAS is the target of five classes of commercial herbicides, including the sulfonylureas, imidazolinones, pyrimidinyl-benzoates, triazolopyrimidines, and sulfonylamino-cabonyl-triazolinones (**Figure 1**). These herbicides capture a major share of the crop-protection market that is valued at more than $USD 30 billion per annum. The popularity of these herbicides amongst farmers is due to their crop selectivity, low toxicity in mammals (LD_{50} rat ~ 5g/kg), and extremely potent herbicidal activity that allows low application rates in the field (~ 10-100 g/ha) [2]. However, resistance to these herbicides is of an increasing concern.After ~20 years of concerted use of these herbicides~50 weed species have been identified to possess target site resistance[3].Thus, a comprehensive understanding of the molecular structure of plant AHAS should provide essential data for the design of next generation herbicides that are less susceptible to target site resistance.

To date, the crystal structures determined for AHAS are*Saccharomyces cerevisiae* (*Sc*) AHAS as the uninhibited enzyme[4], *Sc*AHAS in the presence of six different sulfonylurea herbicides [5, 6] and *Arabidopsis thaliana* (*At*) AHAS in the presence of seven different sulfonylureas and one imidazolinone, imazaquin[7-9]. Comparisons of the structures of *Sc*AHAS in the presence and absence of herbicideshow that the binding of these compounds creates a dramatic effect on the structure of the fungal enzyme.The changesinclude a reduction in the volume of accessible space around the active site, the relative position of FAD and ThDP in the active site and the ordering of a “capping region” (“mobile loop”(Q580-T595) and “C-terminal arm” (P650-H687)) that is critical for herbicide binding [5]. However, the overall amino acid sequences of the plant and fungal enzymes differ considerably and most significantly in the capping regions, opening to question whether or not conformational changes occur to the same extent in *At*AHAS. Also,supporting the concept of a highly flexible herbicide-binding site in plant AHASsis the fact that the crystal structures of *At*AHAS in complex with the sulfonylurea and imidazolinone herbicides show that the amino acid residues in the herbicide-binding site adopt different conformations depending on which class of inhibitor is bound[8].

In the present study we have determined the first crystal structure of the catalytic subunit of a plant AHAS in the absence of any inhibitor and it shows that the polypeptide in the herbicide-binding site has a fold similar to that adopted when the sulfonylureas and imidazolinones are bound to the enzyme. However, a comparative structural analysis shows thatthis site is adaptable through changes to the backbone and side-chain dihedral angles,and that these changes depend on the specific identity of the herbicide that binds. This report therefore provides new insights into the structure of plant AHAS and provides a new starting point for the rational design of new chemical classes ofherbicides that inhibit plant AHAS.

RESULTS AND DISCUSSION

Crystal structure of AtAHAS and comparison with structures of the inhibited enzyme

The crystal structure of free (or uninhibited) *At*AHASwas determined at 2.9 Å resolution(**Table 1**). There is a single monomer in the asymmetric unit with the tetramer generated by crystallographic symmetry(**Figure 2**). Each subunit contains three domains, α (residues 86-280), β (281-451) and γ (463-639), and a C-terminal tail of 22 residues (646-668), all of which have been observed for *At*AHAS in complex with the sulfonylureas and imidazolinones [8].

After fitting ThDP into the electron density a positive peak in the difference map near the C2 carbon atom was observed suggesting the presence of a covalently bound attachment, which we ascribe as the hydroxyethyl (HE) intermediate(**Figure3**).Its appearance in the structure is due to the fact that enzyme was purified in the presence pyruvate and its cofactors, enabling the enzyme to produce ThDP-HE. The strength of the density is indicative of full occupancy. This density feature has also been observed in the crystal structures of *At*AHAS in complex with two monosubstituted sulfonylureas (monosulfuron and monosulfuron ester), though with reduced occupancy[9]. However, in that case pyruvate was not added during purification. Using that purification procedure ~10% of the enzyme (after gel filtration) is active without extra addition ThDP, suggesting that this amount of ThDP-HE is carried through from the expression of the enzyme. Both of theseresults contrast with observations from the *At*AHAS.imazaquin complex [8] and uninhibited*Sc*AHAS [4] that show no attachment to the ThDP, whilethe structures for *At*AHAS in complex with the disubstituted sulfonylureas[8]all show varying degrees of degradation for ThDP. The addition of pyruvate to the purificationhad the additional benefit ofa 2-fold increase in the solubility and amount of the enzyme produced per litre of culture.

The structure of the uninhibited enzyme has an overall fold that is similar to that reported for *At*AHAS when in complex with the sulfonylureas (*e.g.* chlorsulfuron) or the imidazolinone, imazaquin [8].The low rmsd values (0.18 - 0.22 Å for individual subunits, 0.22-0.24Å for the tetramer) when all Cα atoms are superimposed indicate that, overall, the polypeptide backbone and tetrameric structure in thepresence and absence of herbicide does not change significantly (**Figure 2**). Furthermore,analysis of the interactions that stabilize the tetramer are fully conserved when the uninhibited and inhibited structures of *At*AHAS are compared. These highly conserved structures for the plant enzyme werenot anticipated given the structural differences between herbicide bound and uninhibited*Sc*AHAS. Although the polypeptide of *At*AHAS is completely ordered in the uninhibited crystal structure, it is clear that structural adjustments need to be made in order to accommodate the sulfonylurea and imidazolinone herbicides into their respective binding sites. These changes include rotations ofamino acid side-chain torsion angles (*chi* angles), principally involving six residues (R199,M200, K256, D376, R377 and W574) critical for forming direct interactions with the herbicide [8], and changes to many of the backbone (Φ and Ψ) dihedral angles throughout the entire enzyme (**Table 3**).

*Changes to the torsion angles of amino acid side-chains in the herbicide-binding site.*The binding of the sulfonylurea, chlorsulfuron,produces dramatic changes to theside-chains dihedral angles of R199, M200, R377 and W574(**Figure 4A, Table 2**).These rotations provide space for the 2-chlorophenyl moiety of chlorsulfuron to fit into its location and to allow insertion of the heterocyclic ring. The rotation of W574correlates with a movement of the atoms inthe indole ring by up to ~2 Å compared to their positions in uninhibited *At*AHAS (**Figure 4A and C**). This side-chain adjustment is the most important for sulfonylurea binding because it anchors the herbicide via a π stacking interaction that occurs between the heterocyclic ring and the aromatic ring of W574. Accordingly, W574S/L substitutions

increase the inhibition constant(K_i) values by up to 10000-fold [10]. The changes induced at R199 vary depending on which sulfonylurea is bound to *At*AHAS.When chlorsulfuron binds, the side chain of R199 rotates to stabilize at least one water molecule that is hydrogen bonded to an oxygen atom of the sulfonyl group (**Figure 4A**). Three other sulfonylureas (*i.e.* tribenuron-methyl, monosulfuron and monosulfuron-ester) adopt the same orientation as when chlorsulfuron is bound, but when chlorimuron-ethyl, metsulfuron-methyl and sulfometuron-methyl are bound this side-chain moves to adopt different conformations. The orientation of R199 is highly reliant on the polar contacts to the different sulfonylureas and how they interact with other residues of the herbicide-binding site and with the solvent. However, when chlorimuron-ethyl is bound, this water molecule is absent and the R199 side-chain rotates away from the herbicide-binding site.

When the sulfonylureas bind to R377 its side-chain rotates and up to fivepolar interactions (four for chlorsulfuron; **Figure 4A**) are formed. To attain these interactions thisside-chain moves towards the oxygen of the urea bridge and towards the heterocyclic ring.The position of the side-chain of K256 is also influenced by herbicide binding. In the uninhibited enzyme the side-chain adopts two conformations that would partially overlap with the location where the sulfonylurea binds. In the *At*AHAS.chlorsulfuron complex the Nζ atom moves away to allow the herbicide to bind. However, when chlorimuron-ethyl and tribenuron-methyl bind this atom forms a hydrogen bond with one of the sulfonyl oxygen atoms. The side-chain of D376moves in concert with the side-chain of R377, but does not appear to contribute directly to herbicide binding.

There is only one structure of plant AHAS with an imidazolinone bound, that being imazaquin. Compared to their positions in uninhibited *At*AHAS, the three most significant side-chain conformational changes induced by the binding of imazaquinoccur toM200, D376

and R377 (**Figure 4B, Table 2**).. Based on the uninhibited structure, the side-chains of R199, K256 and W574 are already in a favourable location to permit the binding of imazaquin usinghydrophobic interactions.

*Changes to backbone dihedral angles (Φ and Ψ).*Not only do the sulfonylureas and imidazolinones induce changes tothe side-chains dihedral angles of several residues in the herbicide-binding site, they also influence the position of other residues that assist in shapingthe herbicide-binding site by modifying backbone dihedral angles. In total, five sections of the polypeptide are influenced by the presence of herbicide binding(P119-M124, G194-E208, D376-V378, L568-E575 and G654-G655) (**Table 3**).

Major changes to the backbone dihedral angles of I201 and G202occur whenchlorsulfuron binds. Even though these two amino acids do not interact with the herbicide, their backbone atoms provide the necessary flexibility to allow A205 and F206 to moveby~0.7 Å to make contacts with the two aromatic rings of the herbicide (**Figure 4C**). The adjustments in the other nearbyresidues (**Table 3; Figure 5A**)are less pronounced but doinfluence the secondary structure of the loops that constitute the herbicide-binding site.This exemplifies the fact that the sulfonylureas can induce changes to the enzyme that are distal to the herbicide binding site and these assist in maximizing the number of contacts to the herbicide(>50)[8].

The binding of imazaquinproduce changes tothe backbone dihedral angles of 27 amino acid residues nearby to where this herbicide binds (**Table 3**). This analysis show that although imazaquin forms only half of the number of van der Waals interactions (~28 contacts) compared to the sulfonylureas[8], they stillproducesignificant modifications to the herbicide-

binding site.The effect of imazaquinon the secondary structure close tothe herbicide-binding site is different to that observed when the sulfonylureas bind.For example, the backbone dihedral angle changes observed betweenR198 and T203leads to the movement of T203, D204 and A205 by 0.6-1.0 Å and induce the formation of a small α-helix that is not present in uninhibited *At*AHAS, whilethe region between residues D376 and T379 in the uninhibited enzyme and in all of the sulfonylurea complexes isα-helical, but is a random coilin the imazaquin bound structure (**Figure 5B**).

The binding of the sulfonylureas and imazaquinexert a markedly differenteffecton thestructural order of the loops that make up the herbicide-binding site.Analysis of the temperature factors of the *At*AHAS structures show the herbicide-binding site, especially the mobile loop and the C-terminal arm, becomes significantly morerigidin the presence of chlorsulfuron(**Figure5A**). On the other hand,the B-factor values of the capping region are similar in uninhibited *At*AHAS and when imazaquin binds (**Figure 5B**), which suggests that this herbicidedoes not produce as large aneffect on ordering the loops as does the sulfonylureas.In effect, the binding of imazaquin only results inthe ordering of theP119-M124 and G194-E208 loops, both of which are from the neighbouring subunit.

These results show that the herbicide-binding site in plant AHAS is highly adaptable and that sulfonylureas and imidazolinones bind to the enzyme bysignificantly different mechanisms of induced fit. This study also explains how it is possible that herbicides with markedly different chemical structures (*e.g.* sulfonylureas and imidazolinones) can bind to a common site in AHAS.

Comparison of the uninhibited AtAHAS and ScAHAS crystal structures

Superposition of the uninhibited *At*AHAS and *Sc*AHAS (subunit B) gives an overall rmsd of 1.02Å for 410Cα atoms. However, two regions are not superimposable. These are the two elements of the capping region: the mobile loop and the C-terminal arm (**Figure 6;** residues L568-R583 and H646-R667). The mobile loop in*At*AHAS adopts a well-defined α-helix that buries the majority of the atoms in ThDP providing solvent access only to the C2 carbon atom of this cofactor (**Figure7A**). However, this region in uninhibited *Sc*AHAS is an antiparallel β-sheetthat exposes the entire thiazolium ring of ThDP to the solvent(**Figure 6B** and **Figure7B)**. The second element of the capping region, the C-terminal arm, which adopts a U shaped random coil conformation in uninhibited*At*AHAS is disordered in uninhibited *Sc*AHAS.Here we identify several structural features that are different in the two uninhibited enzymes and are responsible for the ordering of the capping region in *At*AHAS.

*Prolyl cis-peptide bonds.*In uninhibited *At*AHAS there is a prolyl *cis*-peptide bond between L648 and P649, a feature that is also present in the structures of both *At*AHAS and *Sc*AHAS in complex with the herbicides, but is absent in uninhibited *Sc*AHAS. Due to the fact P649 is highly conserved across several species of AHASs from plant, fungi and bacteria [1] it has been hypothesized that changingthe conformation of the L648-P649peptide bond from *trans* to *cis*is a crucial step for ordering the C-terminal arm of the polypeptide andthat this regioncreates part of the substrate access channel during catalysis (**Figure6**)[8]. This feature suggests that the *cis*-peptide bond in this location may also be important for herbicide binding since the active and herbicide-binding sites are partially overlapping. A second prolyl *cis*-peptide bond between residues F598 and P599 is identified in uninhibited *At*AHAS,which is located at the end of a loop (residues F587-P599) that has the form of an appendix that protrudesfromthe γ-domain (**Figure6B**). The orientation of this “appendix loop”is attributed to the presence of the *cis*-peptide bond. As a result, interactions are

formed between the appendix loop and the mobile loop. These interactions appear to be critical for stabilization of this region in the absence of herbicide.

*High conservation in the capping region.*A sequence alignment performed on AHASs from plant, fungi and bacteria revealed that the residues of the capping region are highly conserved within plant enzymes (including those from crops and weeds). However, these are markedly different when compared with yeast and bacterial enzymes (**Figure 8**). Several highly conserved residues from the mobile loop and the C-terminal arm of plant AHAS form key interactions that induce the formation of a well-defined secondary structure in the absence of any herbicide. These interactions are mainly formed between residues from the two elements of the capping region(**Figure 9**), which suggest that if any one of thesebecomes ordered the other element will also be ordered.This ordering clearly occurs in*At*AHAS.

*Role of H567.*Analysis of the uninhibited *At*AHAS and *Sc*AHAS structures shows that the divergence in the secondary structure of the mobile loop begins at H567 (E579 in *Sc*AHAS) (**Figure 6B**). The side-chain atoms of this residue form interactions with the side-chain of H643situated just before the start of the C-terminal arm (**Figure9A**). Both H567 and H643 are highly conserved residues in plant AHASs (**Figure 8**) suggesting these residues are critical for maintaining the integrity of the capping region. We observe that the side-chains of F458, R667, Q644, H643, and H567 form a five membered stacking array (each,in turn,separated by 3.4 – 3.8 Å), and this seems to not be coincidental as all five residues are highly conserved across plant AHASs. These interactions play an important role by fixing the C-terminal arm to the core of the protein (**Figure9B**). Moreover, the structure of uninhibited *At*AHAS shows that Q566 and H567 are wrapped in a cavity moulded by the appendix loop (F587-P599) resulting in several hydrophobic interactions not present in *Sc*AHAS. As

described above, H567 is the pivot point where the mobile loop could pass from an ordered to a disordered state. Hence, due to the position of the appendix loop, it is likely that its role is not only linked to maintaining the secondary structure of the mobile loop, but also has other functions. In*Sc*AHASasimilar His-His cationic stacking interaction occurs *only* when the herbicide is bound, recalling the fact the in the free structure the capping region is disordered. The two histidine residues that play this role in *Sc*AHAS areH599 and H687. These are in close structural proximity to where H567 and H643 in *At*AHAS are located, but are not in precisely the same positions in terms of their three-dimensional structure and relative locations in the sequence alignment (**Figure 8**). This further suggests that thistype of association is key for ordering the capping region.

*Role of L568.*L568 forms a large number of hydrophobic contactswith a part of the surface of the enzyme that includes G539, Y118, P119, M513, G539, V571 and L588, all of which are highly conserved in all AHASs[1].The corresponding residue to L568 in *Sc*AHAS is Q580 and it points towards the solvent in the free enzyme structure of *Sc*AHAS, adopting the position of L568 only when the herbicidesare bound. A second role for L568 is to stabilize the binding of the thiazolium ring of ThDP to the enzyme through eight hydrophobic contacts.

*Role of D576.*D576 forms a hydrogen bond with H646 further assisting with the attachment of the C-terminal arm to thehelix in the mobile loop (**Figure 9A**). D576 also interacts with R583 (ionic bond) helping to stabilize this region of the enzyme. With the helix of the mobile loop in place the position of W574 (**Figure9A and 9B**) is stabilized and ready to bind the heterocyclic group of either the sulfonylurea or the imidazolinone herbicides (**Figure 4**).

Role of S653, R577, V648, and *I661.*S653 is located in the C-terminal arm and makes a close association, 3.2-3.5 Å, withthe side-chain of R377 (**Figure 9B**). However, these residues separate from each other upon herbicide binding (**Figure4**).R577, V648, and I661 form a hydrophobic cluster bringing the C-terminal arm and the mobile loop together(**Figure9B**).

This study shows that the plant enzyme appears ready to receive herbicide through a preformed channel without requiring the large conformational changes observed when the sulfonylurea herbicides bind to*Sc*AHAS. This was confirmed by diffusing chlorimuron ethyl into already existing crystals of uninhibited *At*AHAS. The X-ray structure from this sample at 2.5 Å resolution showed that the herbicide binds to the herbicide-binding site and adopts the same conformation as observed in a co-crystallization experiment. This is in contrast to *Sc*AHAS, wherediffusion of the herbicide into the free *Sc*AHAS crystals did not show interpretable electron density for the herbicide nor ordering of the capping region [5].

Why some herbicides are not potent inhibitors of ScAHAS

The crystal structures of *Sc*AHAS in complex with sulfonylureas [5, 6]and *At*AHAS in complex with sulfonylureas and the imidazolinone, imazaquin [8], showed that in general the herbicide-binding site in the two enzymes is similar. The key residues involved in the majority of the interactions that anchor inhibitors from both families of herbicides to the enzyme are highly conserved. However, several questions emerge as to why some of these herbicides are potent inhibitors of *At*AHAS, but are extremely weak inhibitors of the yeast enzyme. One example is the markedly different inhibition that the imidazolinones exert in these enzymes. While several imidazolinone herbicides inhibit *At*AHAS with K_i values in the µM range, the K_i values are in the mM range for *Sc*AHAS [10, 11]. It has been suggested

that two important differences between the plant and yeast AHAS could be responsible for such a disparity in their inhibition by imidazolinones [12]. One refers to the position the C-terminal arm and includes S653, which in *At*AHAS is important for imidazolinone binding. In *Sc*AHAS, this segment of the polypeptide is located ~3 Å further from the expected position the imidazolinone molecule would bind in the herbicide-binding site, which means that no equivalent interactions would form. In agreement with this observation, the serine residue at this position is substituted by G657 in the yeast enzyme, mimicking a common mutation that increases the insensitivity of weeds to the imidazolinones [3]. The other difference is that R199 is replaced by S194 in *Sc*AHAS, which is part of the herbicide-binding site. The G657A substitution produced a6- to 14-foldimprovement in the inhibition of *Sc*AHAS by the imidazolinones imazaquin, imazapyr and imazethapyr, whereas the substitution S194R did not show any effect on improving inhibition [11]. This shows that individual mutations in the *Sc*AHAS herbicide-binding site are not sufficient to significantly enhance the binding of imidazolinone to*Sc*AHAS to a level similar to that observed when these herbicides bind to *At*AHAS. This suggests that the high degree of conservation of residues in the capping region in the plant enzymes play an important role in the binding of imidazolinones (**Figure 8**).

Dimeric ScAHAS vs tetrameric AtAHAS

In all of solution and structural studies to date *Sc*AHAS is a dimer, and*At*AHAS is a tetramer [13, 14]. The reasons as to why they are different are unknown since the active site of AHAS is formed from only two subunits, so the dimer appears sufficient for an active enzyme. Furthermore, there is no indication of co-operativity between the subunits in the plant enzyme. This suggests the tetramer may be formed to enhance stability or solubility of the enzyme. Other ThDP-dependent enzymes, including *Escherichia coli*glyoxylate carboligase(*Ec*GCL)and *Lactobacillus plantarum*pyruvate oxidase(*Lp*POX) are also

tetramers, again with the dimer as the minimum unit for enzyme activity. Examination of the *At*AHAS crystal structures shows there are several key interactions at the tetramer interface. These are present as hydrophobic patches mixed with some polar contacts along the interface area, a pattern generally known to stabilize protein-protein interfaces [15]. Of particular interest are three regions of the polypeptide chain located in the α and β-domains, which participate in the majority of the tetramerinterface interactions. Two of these regions, R198-G202 and R272-K282 from the different dimers form a hydrophobic patch. This is repeated in the two halves of the tetramer four times (**Figure 2**). Ionic contacts involve R272, E227, D230, K282 and E383 (**Figure10A**) with these residues defining the limits of the hydrophobic patch. P274, G275 and S274 form hydrophobic interactions with R198 and R199, which are located at the entrance of the active site. An α-helix comprised by residues E285-E298 at the N-terminus of the β-domain completes the tetramer interface. This segment of the polypeptide and its counterpart from the adjoining dimer are almost orthogonal to each other. Amongst the numerous interactions, a stacking interaction occurs between H288 and H408 and a salt bridge between R294 and E298 (**Figure 10B**).

Large structural differences are observed in the equivalent regions of *Sc*AHAS that help to explain howthis enzyme forms dimers. In *Sc*AHAS, N271-R279 which correspond to Y276-P284 in *At*AHAS are completely disordered, a factor that may not be favourable for forming a tetramer. Secondly, the α-helix formed by the residues S278-A299 at the N-terminus of the β-domain is eight residues longer than in the same region in *At*AHAS (E285-E298) and would createsteric clashes with the T382-K387 region from the adjacent polypeptide chain.

Comparison of ThDP and FAD binding in AtAHAS and ScAHAS

ThDP and FAD bind to uninhibited *At*AHAS by virtue of numerous interactions formed with the polypeptide. Comparison of the structures of uninhibited *At*AHAS and *Sc*AHAS shows a number of similarities and differences in the binding of these two cofactors. In both cases, ThDP is located in the heart of the active site between residues at the dimer interface. The diphosphate tail anchors the cofactor to the enzyme by forming interactions with the magnesium ion, and several highly conserved residues of the gamma domain, H488, D538, S540, N565 and H567. The pyrimidine and thiazolium rings adopt a V-conformation around a highly conserved methionine (M513 in *At*AHAS and M525 in *Sc*AHAS) that protrudes from the protein surface. This cofactor is bent at the C7' atom which connectsthe two heterocyclic rings. In both enzymes, the pyrimidine and thiazolium rings are almost orthogonal to one another forming an angle of 112°. It has been shown this conformation is essential for cofactor activation since it approaches the C2 carbon atom at 3.1 Å from the 4'-amino nitrogen of the pyrimidine ring, a distance that facilitates proton transfer at C2 [16]. The pyrimidine ring is locked in position by polar interactions formed withthe conserved residues E144 and G511 (E139 and G523 in *Sc*AHAS). The dihedral angles of the pyrimidine (Φ_P) and the thiazolium (Φ_T) rings in uninhibited *At*AHAS are -64° and 106°, respectively, which are similar values to that observed in uninhibited *Sc*AHAS (Φ_P = -66° and Φ_T = 96°). These features show that the binding mode and conformation adopted by ThDP aresimilarin plant and yeast AHASs. Thus, in the presence or absence of the "ordered" mobile loop (**Figure 7**), the binding mode of ThDP remains the same.

The structure of uninhibited *At*AHAS shows H567, G569, M570and V571 provide a large surface area that encircles the atoms of the phosphate tail and the thiazolium ring of ThDP. In uninhibited *Sc*AHAS water molecules take the position of these residues, which results in a large decrease in the number of interactions between the enzyme and ThDP as well as a

translation of the position of this cofactor. In uninhibited *At*AHAS, ThDP form 14 hydrogen bonds and ~100 van der Waals interactions, whereas only 10 hydrogen bonds and ~70 van der Waals interactions are observed for this cofactor in the yeast AHAS structure[4]. It has been shown that theK_m of ThDP for*At*AHAS and *Sc*AHAS are 25 μM [10], and 110 μM [17], respectively, values that correlate with the structural differences we observe in the two uninhibited enzymes.

In both enzymes, FAD is in the extended conformation with the flavin ring located in the active site with the methyl groups pointing towards the C2 atom of ThDP, and this cofactor interacts with a similar number ofamino acid residues. However, the flavin ring adopts a different position in the two enzymes (**Figure 11**) caused by the different conformations adopted by the nearby side-chains(*i.e.*H352, M351 and R377). In uninhibited *At*AHAS, the position of these residues is strongly influenced by the ordering of the residues from P649 to S653 of the C-terminal arm,all of which interact with the residues that make up the flavin-binding site.As a result, the C7 atom of the isoalloxazine ring is at 6.1 Å from the C2 atom of ThDP in *At*AHAS, but 9.1Å from the C2 atom in *Sc*AHAS. The result of this difference is that there is an enlarged volume in the active site of the uninhibited *Sc*AHAS.

Comparison with other ThDP dependent enzymes

Previously, AHAS hasbeen compared with pyruvate oxidase (POX) and benzylformate decarboxylase (BFDC) due to their structuralsimilarities and similar cofactor requirements. However, a current search of the PDB shows that there are other enzymes whose structure resembles AHAS.Ten classes of ThDP-containing enzymes were found to have a similar secondary structure to*At*AHAS.The majority of these enzymes are FAD-independent, which suggests the structure adopted by all these proteins is due to ThDP. *Ec*GCL has the highest

similarity with an rmsd of 1.04Å when 416 Cαatomsare superposed, a value comparable with the rmsd observed between *At*AHAS and *Sc*AHAS (1.02 Å for 410 Cα atoms), and consistent with the suggestionAHAS and GCL are evolutionarily related[18]. TheAHAS ancestor enzyme, *Lp*POX[19] also has a high similarity with an rmsd value of 2.16 Å for 383 Cαatoms.The superposition of uninhibited *At*AHAS with *Ec*GCL and*Lp*POXshowsthe majority of the polypeptide overlaps; however, in *Lp*POX the orientation and organization of the α and β-domains are significantly different, especiallywith regard to the loops contouring the FAD-binding site. Even though the reaction catalyzed by the three enzymes is related, POX is the only one that catalyzes a net redox reactionthat involves the transfer of electrons via FAD [20].Hence,the structural differences observed in the FAD-binding site between AHAS, GCL and the ancestor enzyme are probably due to the divergence of their catalytic activities during evolution and the role FAD plays in each reaction. The crystal structure of *Ec*GCL contains a U-shaped C-terminal overlapping the position of this region in *At*AHAS.The only difference is that*Ec*GCL contains 20 additional residues forming a loop covering a surface of the β and γ-domaininterface. This was somewhat anticipated since both enzymes are evolutionarily related and catalyse similar reactions. Nonetheless, when comparing this section of the polypeptide with the correspondent region in *Lp*POX, the differences are markedly pronounced. In *Lp*POX the C-terminal tail consists of two loops and twoα-helixes covering the substrate access channel in a totally different fashion. There are no obvious reasons to explain as to why the C-terminal tail in the ThDP-dependent enzymes adopt one or another conformation. In AHAS, besides its critical function during catalysis and herbicide binding, it has been hypothesized that the C-terminal arm could constitute part of the regulatory subunit-binding site, though this is yet to be confirmed.

The five commercial herbicide families were initially developed in the absence of any structural information. These chemicals were largely developed on the back of progressive improvements in herbicidal activity. Here we show that uninhibited*At*AHAS adopts an

ordered conformation in the crystalline state that is similar to that observed when either the sulfonylurea or imidazolinone herbicides are bound, but neither is truly reflective of the precise structure of the uninhibited enzyme.The presence of an ordered capping region, mobile loop and herbicide binding site in this crystal structure was somewhat surprising given that these regions are disordered in the crystal structure of uninhibited *Sc*AHAS. An analysis of the crystal packing for *At*AHAS shows that these regions are at least 8 Å away from any symmetry neighbour suggesting that crystal packing does not affect the fold of this protein. On the other hand, in the uninhibited *Sc*AHAS crystals with two molecules per asymmetric unit, the capping region and herbicide binding site of one subunit is partially visible and makes close contacts with symmetry neighbours (possibly influencing the fold). However, in the other subunit this region is completely invisible. But if it were visible, it would be in a position remote from where any crystal packing contacts could form. Thus, if the mobile and capping region were even marginally stable then this site would provide the opportunity for folding. Further solution studies are required to complete clarify this conclusion, which we base solely on the currently available crystal structures. This investigation shows that the conformation of residues both nearby and remote from the herbicide binding site adapt to bind the different chemical classes of herbicides. Such information is a significant advance as these differences are unlikely to be detected by computational molecular modelling based on the herbicide bound structures. Thus, the knowledge of thecrystal structure of uninhibited *At*AHAS represents a fundamental advance as it opens new pathways for rational structure based inhibitor design.

MATERIALS AND METHODS

Protein expression and purification

The construct to express the catalytic subunit of*At*AHASin *E. coli* BL21 (DE3) cells was described previously [7]. For this experiment, a single colony of *E. coli* BL21 (DE3) cells containing the plasmid for *At*AHAS was grown overnight at 37°C in 100 mL of Luria-Bertani (LB) media supplemented with kanamycin (50 μg/mL). 40 mL of this culture was transferred to 1L of Terrific Broth (TB) supplemented with kanamycin (50 μg/mL), and incubated at 37°C with shaking (150 opm). When the OD_{600} reached 2.0, expression of AHAS was induced with 0.5 mM IPTG, and cells were further grown for 18 h at 15°C with shaking (150 opm). Cells were collected by centrifugation at 5000 rpm for 20 min, and the cell paste was snap frozen in liquid nitrogen and stored at -70°C. All subsequent steps were performed at 4°C and protecting the enzyme from light for as much as possible. The cell paste was thawed and resuspended in 50 mM Tris pH 7.9, 1 mM ThDP, 10 mM $MgCl_2$, 500 mM NaCl, 10 μM FAD and 5 mM imidazole (Binding buffer). For lysis, 10 mg of lysozyme per gram of cell, 50 μL of DNase (50 μg/μL) and 1 protease inhibitor cocktail tablet (Complete™, EDTA-free from Roche) were added. The cell suspension was incubated on ice for 15 minutes and then sonicated in a Branson Sonifier 250 for 12 X 10 s at constant duty cycle, with rest intervals of 10 s. The cell debris was removed by centrifugation at 18000 rpm for 60 min. The supernatant was loaded onto a Ni-NTA resin (Qiagen) previously equilibrated with binding buffer, using an ÄKTAprime plus FPLC (GE). After the supernatant was loaded, the column was washed with sixcolumn volumes of 50 mM Tris pH 7.9, 1 mM ThDP, 10 mM $MgCl_2$, 500 mM NaCl, 10 μM FAD and 20 mM imidazole (wash buffer). The enzyme was then eluted with five column volumes of 50 mM Tris pH 7.9, 1 mM ThDP, 10 mM $MgCl_2$, 500 mM NaCl, 10 μM FAD and 400 mM imidazole (elution buffer). The flow throw was collected in 2 mL fractions. The fractions containing enzyme were pooled and incubated with 50 mM pyruvate during 10 min on ice. The enzyme was then loaded onto a S-200 HR gel filtration column

(Pharmacia) previously equilibrated with 50 mM Tris pH 7.0, and 10 μM FAD (GF buffer). The enzyme was eluted with 400 mL of the same buffer with the flow throw collected in 5 mL fractions. The fractions containing enzyme were pooled and concentrated using an Amicon concentrating device. The purified enzyme was stored in aliquots of 30 μL at -70°C. All chemicals used were of analytical grade, and were purchased from Sigma-Aldrich, unless otherwise stated. Protein concentration was measured with Direct Detect™ system (Millipore).

Protein crystallization and structure determination

Crystallization trials were performed using the hanging-drop vapour-diffusion method as described previously [7]. The protein solution was prepared by incubating freshly thawed enzyme (40 mg/mL) with 5 mM $MgCl_2$, 1 mM ThDP, and 1 mM FAD. Crystals were obtained by mixing well solution and protein solution in a 1:2 ratio. The well solution contained 1 M sodium potassium tartrate, 0.1 M CHES and 0.1-0.2 M lithium sulfate. The pH of the solution that yielded crystals ranged from 9.4 to 9.8. The crystallization experiments were conducted at 290 K, and were protected from light by wrapping the trays in foil paper. For cryocooling the crystals were transferred to a drop containing well solution and 35% v/v ethylene glycol, andcofactors at 1 mM concentration. The crystals were mounted in nylon loops and cryocooled in liquid nitrogen.

X-ray data were collected using the MX1 beam line at the Australian Synchrotron, operated at 13 keV, and using an ADSC QUANTUM 210r detector. The data sets were indexed, integrated and scaled using HKL-2000 [21]. The structure was solved by molecular replacement with PHASER [22] using the crystal structure of *At*AHAS in complex with metsulfuron-methyl as the model (PDB code 1YHY). Model building was carried out using

Coot 0.8.1[23] and refinement using Phenix 1.9–1692[24]. The electron density maps also showed a molecule of 2-(*N*-cyclohexylamino)ethanesulfonic acid (CHES) from the crystallization buffer in the asymmetric unit. This molecule is remote from the active and herbicide-binding site and is not likely to influence the structure. C340 was modified to its sulfonic acid derivative as observed when herbicide is bound[8, 9]. Thus, the presence of the herbicide does not influence the oxidation state of this residue. Figures were generated with CCP4mg [25] and PyMOL [26].

Sequence alignment

The amino acid sequences for the catalytic subunit from ten plants, four fungi and five bacteria were obtained from NCBI and were aligned using Clustal Omega [27]. The colouring of the alignment output file was carried out using BoxShade.

Protein structure comparison

The 3-D coordinates file of the uninhibited *At*AHAS structure was compared with all entries in the PDB database using PDBe FOLD based in secondary structure matching (SSM) [28].

AUTHOR CONTRIBUTIONS

M.D.G., J.G.W., T.L., L.W.G. all contributed to the measurement and analysis of data, and to the preparation and writing of the manuscript.

ACKNOWLEDGEMENTS

The initial crystallographic conditions were determined using the Mosquito and Rock imager facilities at the University of Queensland Remote-Operation Crystallization facility (UQROCX). Preliminary X-ray data were measured at this facility. We acknowledge the use of the Australian Synchrotron and the University of Queensland Remote-Operation X-Ray (UQ-ROCX) Diffraction Facility. This work was supported by funds with grant number 1008736 from the National Health and Medical Research Council, the Natural Science Foundation of China (No. 21672114) and the National Basic Research Program of China (No. 2013CB734004).

REFERENCES

1. Duggleby, R. G. & Pang, S. S. (2000) Acetohydroxyacid synthase, *J Biochem Mol Biol.* **33**, 1-36.

2. Gutteridge, S., Thompson, M. E., Ort, O., Shaner, D. L., Stidham, M., Singh, B., Tan, S., Johnson, T. C., Mann, R. K., Schmitzer, P. R., Gast, R. E., deBoer, G. J., Yoshimura, T., Hanai, R., Shimizu, T., Müller, K.-H., Gesing, E.-R. F. & Santel, H.-J. (2012) Acetohydroxyacid synthase inhibitors (AHAS/ALS) in *Modern crop protection compounds* (Krämer, W., Schirmer, U., Jeschke, P. & Witschel, M., eds) pp. 29-162, Wiley-VCH Verlag GmbH & Co. KGaA.

3. Yu, Q. & Powles, S. B. (2014) Resistance to AHAS inhibitor herbicides: current understanding, *Pest Manag Sci.* **70**, 1340-1350.

4. Pang, S. S., Duggleby, R. G. & Guddat, L. W. (2002) Crystal structure of yeast acetohydroxyacid synthase: a target for herbicidal inhibitors, *J Mol Biol.* **317**, 249-262.

5. Pang, S. S., Guddat, L. W. & Duggleby, R. G. (2003) Molecular basis of sulfonylurea herbicide inhibition of acetohydroxyacid synthase, *J Biol Chem.* **278**, 7639-7644.

6. McCourt, J. A., Pang, S. S., Guddat, L. W. & Duggleby, R. G. (2005) Elucidating the specificity of binding of sulfonylurea herbicides to acetohydroxyacid synthase, *Biochemistry.* **44**, 2330-2338.

7. Pang, S. S., Guddat, L. W. & Duggleby, R. G. (2004) Crystallization of *Arabidopsis thaliana* acetohydroxyacid synthase in complex with the sulfonylurea herbicide chlorimuron ethyl, *Acta Crystallogr D.* **60**, 153-155.

8. McCourt, J. A., Pang, S. S., King-Scott, J., Guddat, L. W. & Duggleby, R. G. (2006) Herbicide-binding sites revealed in the structure of plant acetohydroxyacid synthase, *Proc Natl Acad Sci USA.* **103**, 569-573.

9. Wang, J. G., Lee, P. K.-M., Dong, Y. H., Pang, S. S., Duggleby, R. G., Li, Z. M. & Guddat, L. W. (2009) Crystal structures of two novel sulfonylurea herbicides in complex with *Arabidopsis thaliana* acetohydroxyacid synthase, *FEBS J.* **276**, 1282-1290.

10. Chang, A. K. & Duggleby, R. G. (1998) Herbicide-resistant forms of *Arabidopsis thaliana* acetohydroxyacid synthase: characterization of the catalytic properties and sensitivity to inhibitors of four defined mutants, *Biochem J.* **333**, 765-777.

11. Duggleby, R. G., Pang, S. S., Yu, H. & Guddat, L. W. (2003) Systematic characterization of mutations in yeast acetohydroxyacid synthase, *Eur J Biochem.* **270**, 2895-2904.

12. Duggleby, R. G., McCourt, J. A. & Guddat, L. W. (2008) Structure and mechanism of inhibition of plant acetohydroxyacid synthase, *Plant Physiol Biochem.* **46**, 309-324.

13. Pang, S. S. & Duggleby, R. G. (2001) Regulation of yeast acetohydroxyacid synthase by valine and ATP, *Biochem J.* **357**, 749-757.

14. Lee, Y.-L. & Duggleby, R. G. (2001) Identification of the regulatory subunit of *Arabidopsis thaliana* acetohydroxyacid synthase and reconstitution with its catalytic subunit, *Biochemistry.* **40**, 6836-6844.

15. Larsen, T. A., Olson, A. J. & Goodsell, D. S. (1998) Morphology of protein-protein interfaces, *Structure.* **6**, 421-427.

16. Bar-Ilan, A., Balan, V., Tittmann, K., Golbik, R., Vyazmensky, M., Hübner, G., Barak, Z. & Chipman, D. M., , (2001) Binding and activation of thiamin diphosphate in acetohydroxyacid synthase, *Biochemistry.* **40**, 11946-11954.

17. Poulsen, C. & Stougaard, P. (1989) Purification and properties of *Saccharomyces cerevisiae* acetolactate synthase from recombinant *Escherichia coli.*, *Eur J Biochem.* **185**, 433- 439.

18. Chang, Y.-Y., Wang, A.-Y. & Cronan, J. E. (1993) Molecular cloning, DNA sequencing, and biochemical analyses of *Escherichia coli* glyoxylate carboligase, *J Biol Chem.* **268**, 3911-3919.

19. Chang, Y.-Y. & Cronan, J. E. (1988) Common ancestry of *Escherichia coli* pyruvate oxidase and the acetohydroxy acid synthases of the branched-chain amino acid biosynthetic pathway, *J Bacteriol.* **170**, 3937-3945.

20. Tittmann, K., Wille, G., Golbik, R., Weidner, A., Ghisla, S. & Hübner, G. (2005) Radical phosphate transfer mechanism for the thiamin diphosphate- and FAD-dependent pyruvate oxidase from *Lactobacillus plantarum*. Kinetic coupling of intercofactor electron transfer with phosphate transfer to acetyl-thiamin diphosphate via a transient FAD semiquinone/hydroxyethyl-ThDP radical pair, *Biochemistry.* **44**, 13291-13303.

21. Otwinowski, Z. & Minor, W. (1997) Processing of X-ray diffraction data collected in oscillation mode in *Methods in Enzymology* (Carter, C. W. & Sweet, R. M., eds) pp. 307-326, Academic Press, New York.

22. McCoy, A. J., Grosse-Kunstleve, R. W., Adams, P. D., Winn, M. D., Storoni, L. C. & Read, R. J. (2007) Phaser crystallographic software, *J Appl Crystallogr.* **40**, 658-674.

23. Emsley, P. & Cowtan, K. (2004) Coot: model-building tools for molecular graphics, *Acta Crystallogr D.* **60**, 2126-2132.

24. Afonine, P. V., Grosse-Kunstleve, R. W., Echols, N., Headd, J. J., Moriarty, N. W., Mustyakimov, M., Terwilliger, T. C., Urzhumtsev, A., Zwart, P. H. & Adams, P. D. (2012) Towards automated crystallographic structure refinement with phenix.refine, *Acta Crystallogr D Biol Crystallogr.* **68**, 352-367.

25. McNicholas, S., Potterton, E., Wilson, K. S. & Noble, M. E. M. (2011) Presenting your structures: the *CCP4*mg molecular-graphics software, *Acta Crystallogr D.* **67**, 286-294.

26. DeLano, W. L. (2002) The PyMOL Molecular Graphics System.

27. Sievers, F., Wilm, A., Dineen, D. G., Gibson, T. J., Karplus, K., Li, W., Lopez, R., McWilliam, H., Remmert, M., Söding, J., Thompson, J. D. & Higgins, D. (2011) Fast, scalable generation of high-quality protein multiple sequence alignments using Clustal Omega, *Mol Syst Biol.* **7**, 539.

28. Krissinel, E. & Henrick, K. (2004) Secondary-structure matching (SSM), a new tool for fast protein structure alignment in three dimensions, *Acta Crystallogr D.* **60**, 2256-2268.

TABLES

Table 1. Data collection and refinement statistics for *At*AHAS.

Unit cell (Å), a = b, c	178.93, 186.09
Space group	$P6_422$
Diffraction data[a]	
Temperature (K)	100
Resolution range (Å)	44.56-2.95
Observations [I > 0σ(I)]	589,009 (24,669)
Unique reflections [I > 0σ(I)]	37,387 (1,841)
Completeness (%)	99.7 (100.0)
R_{merge}[b]	0.101 (0.907)
R_{pim}	0.034 (0.478)
$\langle I \rangle / \langle \sigma(I) \rangle$	31.3 (2.1)
Refinement statistics	
Resolution limits (Å)	44.56-2.95
R_{factor}	0.1906
R_{free}	0.2291
rmsd[c] bond lengths (Å)	0.002

rmsd bond angles (°)	0.603
Ramachandran plot (%)	
Favoured	97.4
Outliers	0

[a] Values in parenthesis are for the outer-resolution shells: 3.00 – 2.95 Å. [b] $R_{merge} = \Sigma | I - \langle I \rangle | / \Sigma \langle I \rangle$, where I is the intensity of an individual measurement of each reflection, and $\langle I \rangle$ is the mean intensity of that reflection. [c] rmsd, root-mean-square deviation.

Table 2.Changes to dihedral angles residues upon herbicide binding to*At*AHAS.

Chlorsulfuron	
Residue	
M200	17° around chi3
W574	8° around chi1 and 20° around chi2
R199	95° around chi3
R377	90°around chi4
Imazaquin	
M200	180°around chi3
D376	180°around chi1
R377	100° around chi2

Table 3. Changes in backbone dihedral angles upon herbicide binding to *At*AHAS.

Residue	ΔΦ		ΔΨ	
	CS	IQ	CS	IQ
P119	8.1	17.6	7.8	6.3
G120	12.5	9.4	1.9	5.5
G121*	6.1	3.1	22.0	18.7
A122*	22.5	22.4	7.9	10.8
S123	13.5	14.6	9.3	18.1
M124	13.0	19.3	10.3	13.9
G194	9.3	12.6	3.6	17.7
Q195	14.9	29.7	10.8	12.4
V196*	13.0	15.5	8.9	4.7
R198	12.3	15.3	19.4	23.5
R199*	11.0	11.6	3.9	9.0
M200*	14.7	21.8	12.9	12.9
I201	19.2	12.7	24.1	18.9
G202	32.9	27.3	5.9	18.3
T203	6.0	26.5	1.2	19.8
F206*	9.6	16.2	3.2	7.6

E208	11.3	2.3	14.0	17.9
D376*	5.1	1.5	4.6	23.4
R377*	7.8	5.3	17.5	23.9
V378	13.1	16.5	2.6	7.5
L568	12.7	18.6	0.1	8.9
G569	15.9	17.4	15.1	13.8
V571*	1.3	14.4	2.4	10.1
W574*	0.8	4.7	4.3	20.1
E575	6.8	19.9	3.6	3.9
G654*	2.8	9.9	20.7	44.5
G655	21.7	45.5	9.6	2.8
T656	1.0	17.2	19.8	7.0
F657	15.4	14.7	0.3	1.7
N658	4.8	1.0	21.0	8.3
D659	18.4	5.5	12.6	12.2
V660	12.2	13.4	7.1	8.5

* Amino acid residues in *At*AHAS that form interactions with chlorsulfuron (CS) or imazaquin(IQ).

FIGURE LEGENDS

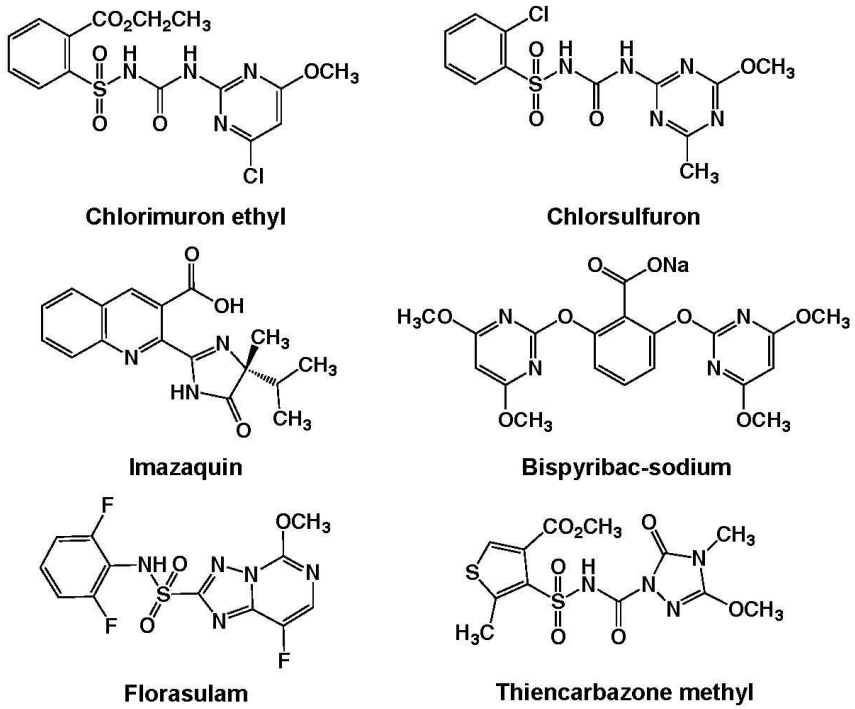

Figure 1. Examples of the chemical structures of the five different classes of AHAS herbicides: sulfonylureas (chlorimuron-ethyl and chlorsulfuron), imidazolinones (imazaquin), pyrimidinyl-benzoates (bispyribac-sodium), triazolopyrimidines (florasulam) and sulfonylamino-carbonyl-triazolinones (thiencarbazone-methyl)**.**

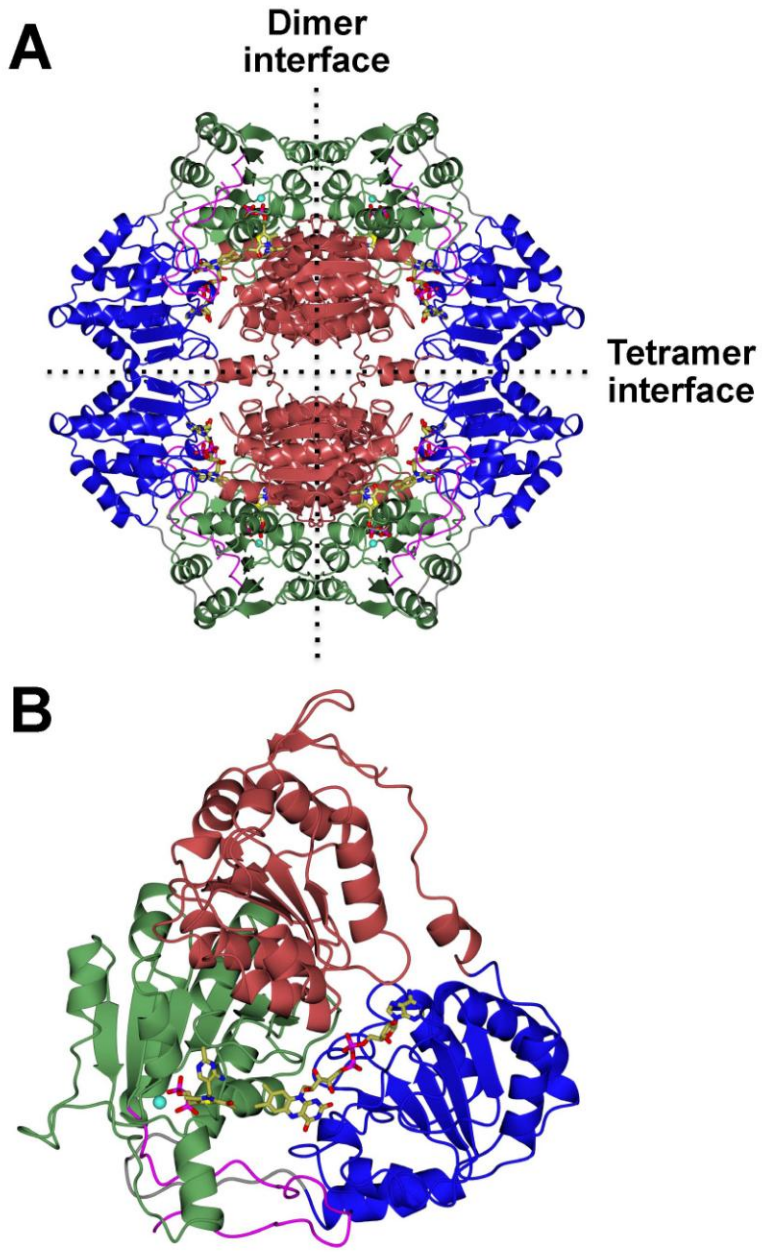

Figure 2.Overall fold of *At*AHAS. (A) The tetramer. (B) A single subunit. The α (86-280), β (281-451) and γ (463-639)-domains are coloured red, blue and green, respectively. The C-terminal tail (640-668) in each monomer is depicted in pink. FAD and ThDP are shown as stick models; carbon (gold), nitrogen (blue), oxygen (red), sulfur (yellow) and phosphorus (magenta). The Mg^{2+} ion is represented as a cyan sphere. Dashed lines highlight the dimer and tetramer interfaces.

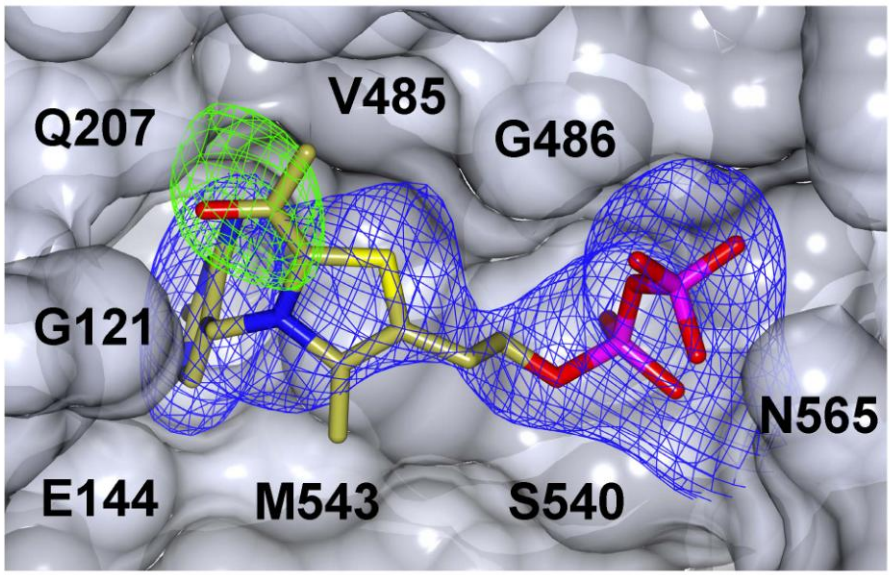

Figure 3.ThDP-HE in the uninhibited *At*AHAS structure.The $2F_o - F_c$ electron density (2.0 σ above the background) after fitting ThDP (alone) is shown in blue. The $F_o - F_c$ difference electron density map contoured at 3.5σ above the backgroundfor this structure is in green. These maps allowed us to ascribed the additional green electron density to the presence of the HE intermediate.

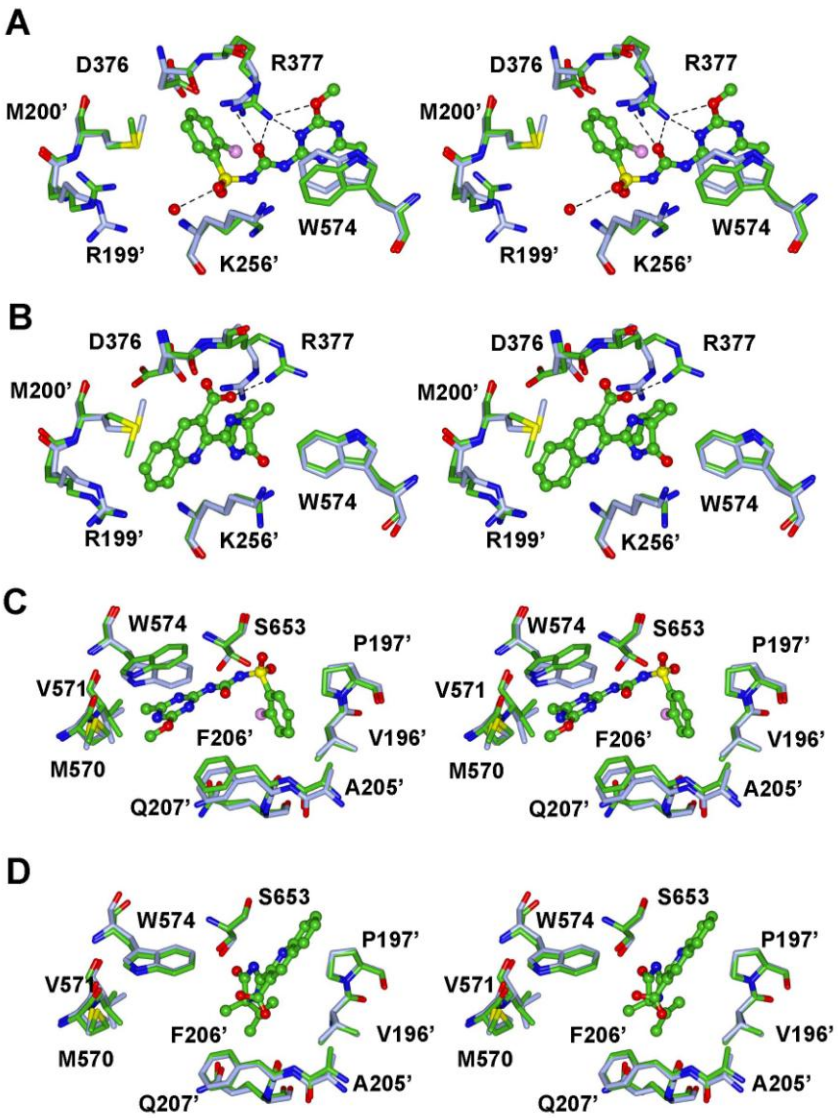

Figure 4. Stereoview of the conformational changes in the *At*AHAS herbicide-binding site. The residues for herbicide binding adopt a different position depending on whether (A) and (C) CS (PDB code 1YHZ) or (B) and (D) IQ (PDB code 1Z8N) is bound to the enzyme. Amino acid residues are represented as stick models and CS and IQ are represented as ball and stick models. The carbon atoms for the free enzyme and the enzyme in complex with herbicide are coloured blue and green, respectively. The colour scheme for the other atoms

is as per Figure 2. Water is shown as a red sphere. The ‘ indicates that these residues are from the neighbouring subunit. Dashed lines represent hydrogen bonds.

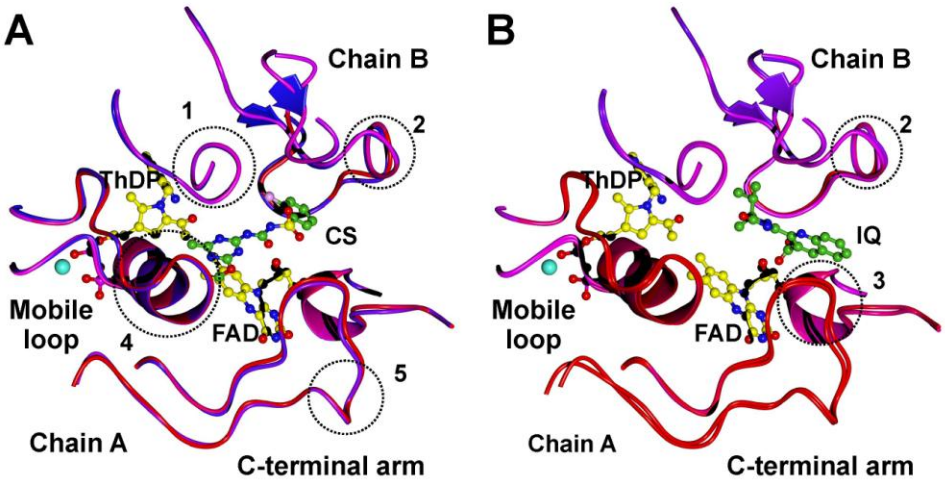

Figure 5. Herbicide binding site of *At*AHAS. Superposition of the uninhibited structure and the complex with (A) CS and (B) IQ. FAD, ThDP (yellow) and the herbicides (green) are represented by ball and stick models. Mg^{2+} is represented as a cyan sphere. Loops are coloured according to B factor (blue low to red high). The regions circled correspond to those in Table 3. (1) P119-M124, (2) G194-E208, (3) D376-V378, (4) L568-E575 and (5) G654-G655.

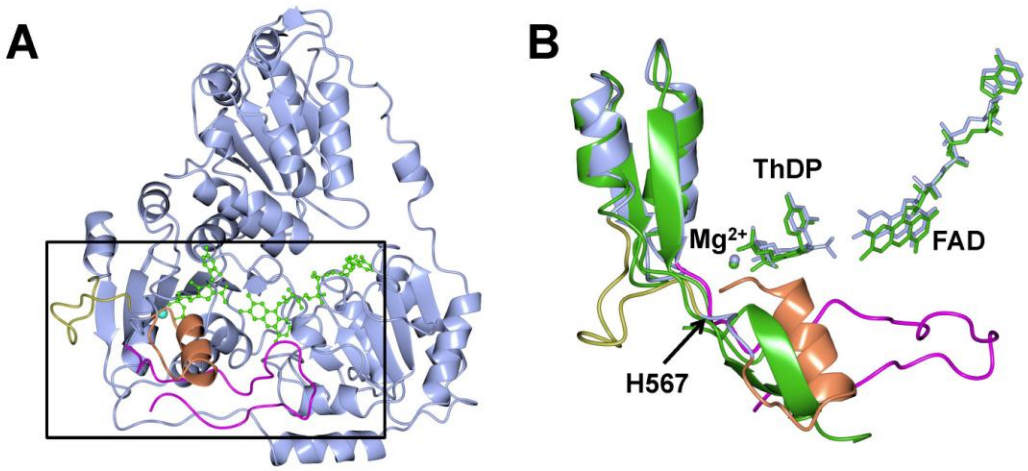

Figure 6. The capping region of *At*AHAS. (A) Overall fold of *At*AHAS with cofactors FAD, ThDP (green ball and stick models) and Mg^{2+} (cyan sphere). The two elements of the capping region, the “mobile loop” (L568-R583) and the “C-terminal arm” (H646-R667) are coloured in orange and magenta, respectively. The appendix loop (F587-P599) present only in *At*AHAS is coloured gold and the rest of the polypeptide is depicted light blue. (B) Part of the gamma domain from uninhibited *At*AHAS (enclosed in (A) with a black square) including the capping region was superimposed with the corresponding region of uninhibited *Sc*AHAS (PDB code 1JSC; green).

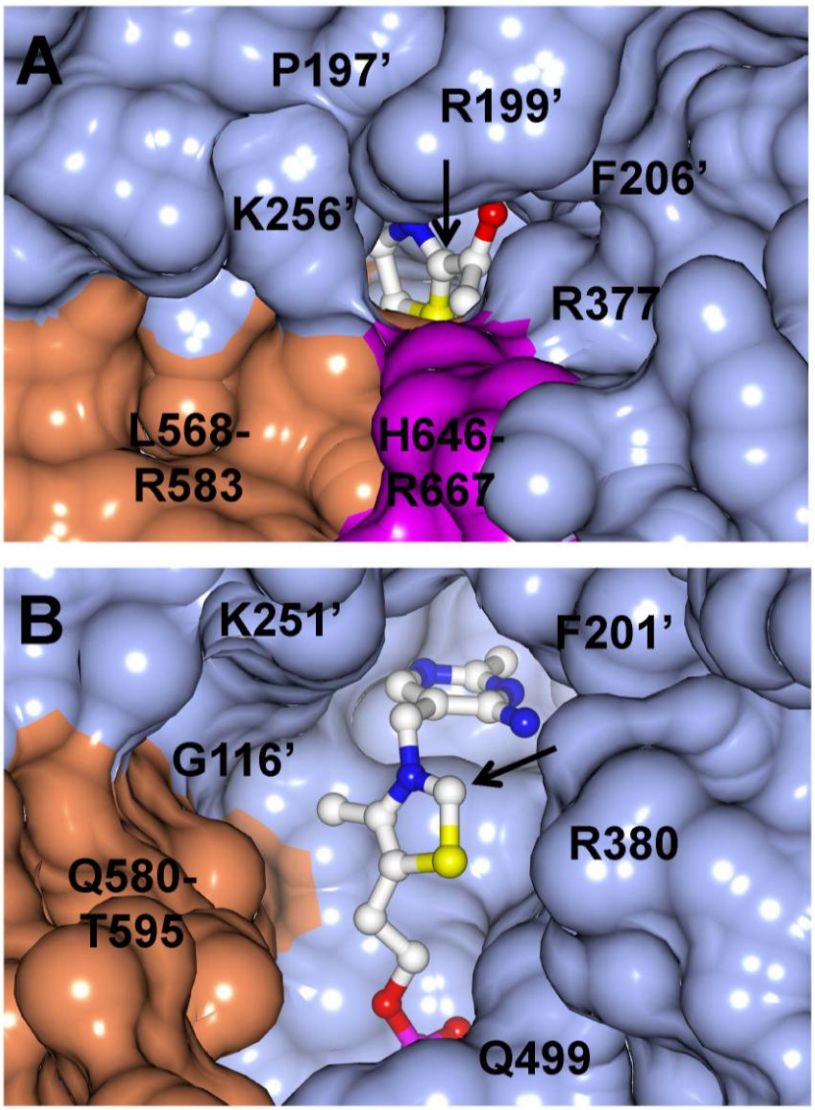

Figure 7. ThDP in the uninhibited *At*AHAS and *Sc*AHAS. Surface representation showing the position of ThDP in (A) uninhibited *At*AHAS and (B) uninhibited *Sc*AHAS. The arrow indicates the position of the C2 carbon atom. The polypeptides are coloured ice blue, except that the "mobile loop" and the "C-terminal arm" are coloured orange and magenta, respectively. ThDP (ThDP-HE in *At*AHAS) is shown as a ball and stick model with carbon, coloured white. The colour scheme for the other atoms is as per Figure. 2. ' indicates that these residues belong to the adjoining subunit.

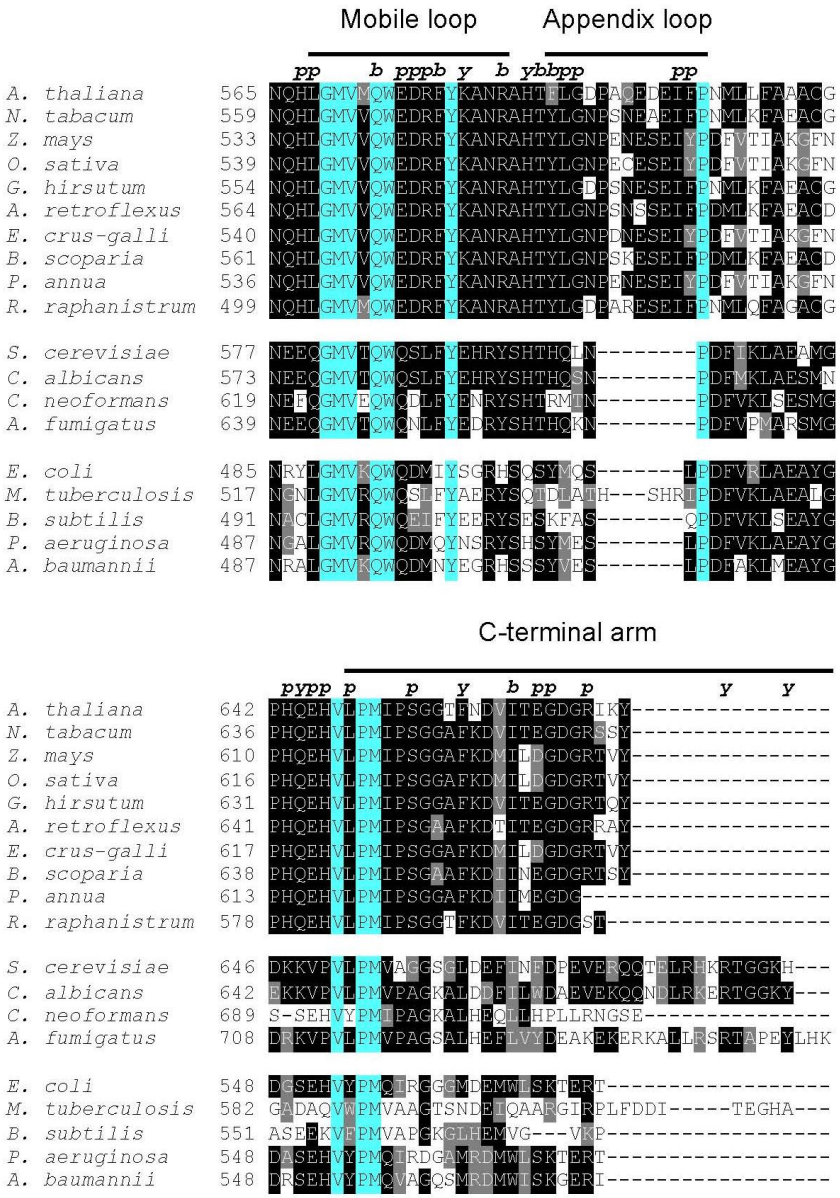

Figure 8.Multiple sequence alignment of the capping region of AHAS from ten plants, four fungi and five bacteria. Residues forming key non-covalent interactions that influence the ordering of the capping region of plant, yeast and both enzymes are labelled *p*, *y* and *b*, respectively. Identical and conserved residues within plant, or within fungal or within bacterial AHASs are highlighted by black and gray shading, respectively, and those identical across AHAS from the different sources are highlighted by cyan shading.

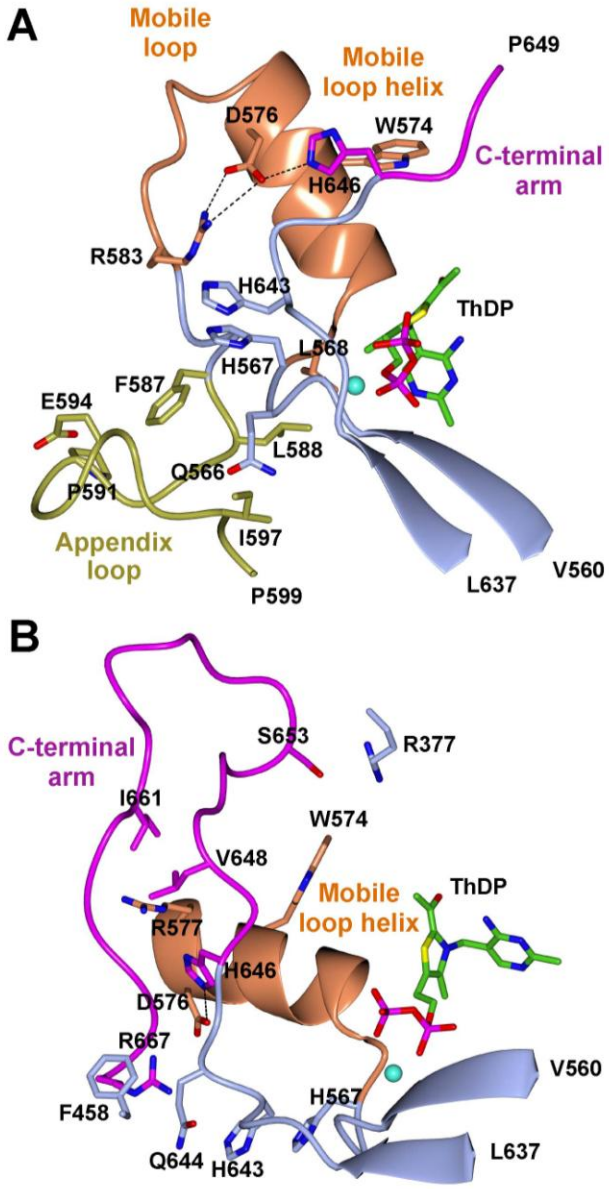

Figure 9. Structure of the capping region of *At*AHAS. (A) The mobile loop and appendix loop. (B) The C-terminal arm.The polypeptide in the capping region is coloured orange (mobile loop), gold (appendix loop) and magenta (C-terminal arm). The remainder of the protein is blue. ThDP and the residues forming key interactions stabilizing the secondary structure of the capping region are represented as stick models, and Mg^{2+} (cyan) is represented as a sphere. The carbon atoms for ThDP are coloured green. The colour scheme for other atoms is as per Figure 2.

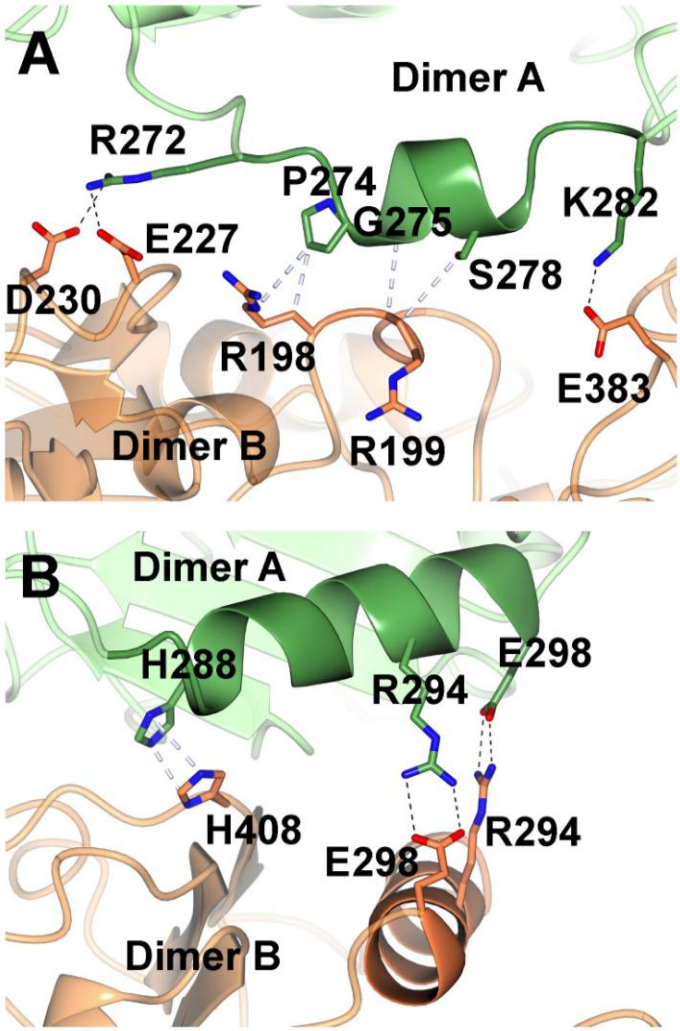

Figure 10. Regions forming the tetramer interface interactions. (A) The R198-G202 loop and the R272-K282 helix, each from different dimers, form a hydrophobic patch repeated four times at the tetramer interface. (B) The E285-E298 helix, and its counterpart from the adjoining dimer. The residues forming key interactions are represented as stick models. Carbon atoms are represented in green for dimer A and orange for dimer B. The colour scheme for the other atoms is as per Figure 2.

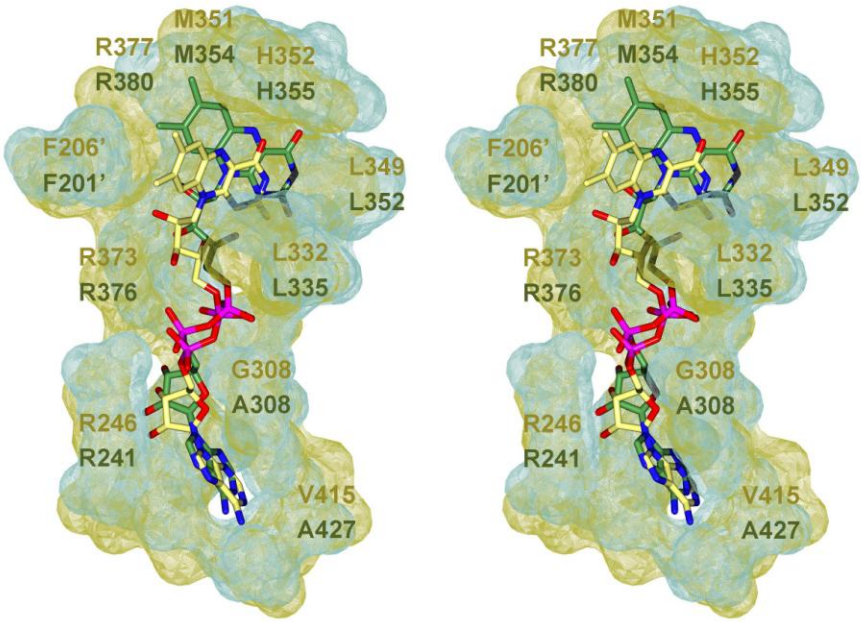

Figure 11. Stereo representation of FAD in uninhibited *At*AHAS and *Sc*AHAS. In both enzymes FAD is in the extended conformation bound to the surface of residues from the three domains. However, the surface of the flavin-binding cavity in *At*AHAS (gold) is significantly different to that observed in *Sc*AHAS (green). The carbon atoms of FAD are coloured lemon (*At*AHAS) and green (*Sc*AHAS). The colour scheme for the other atoms is as per Figure 2.